,,cmrftm

# Contents

# 1 Abstract

Graphene is of interest as the most studied of the two-dimensional materials. In particular, optical measurements were performed on graphene. Ellipsometry was used to obtain the optical constants of graphene. However, this is a model measurement method. To get the optical constants, you must first assign an optical model to the structure. Optical constants are calculated using the parameters that best ensure that the model matches the experiment. In the case of thin film analysis, this method has the following drawback: the noise obtained in the experiment in the data when using optimization procedures, it causes incorrect deviations in the result. This paper describes a different approach to experiment preparation and data analysis. Noise in the data will be suppressed if the ellipsometric map of the sample is measured twice: before graphene transfer to the substrate and after transfer. The resulting difference in ellipsometric data can be calculated analytically if we consider the effect of thin film deposition as a linear perturbation of the reflection and transmission coefficients. This difference will be a function of the desired graphene optical constants. Then, having experimental data with a known error and solving an algebraic equation, it is possible to obtain optical constants with high accuracy. This method is universal and can be applied not only to graphene, but also to other two-dimensional crystals whose thickness is much smaller than the wavelength.

# 2 Literature review

## 2.1 Graphene

Graphene is a promising material for building modern electronic and optical devices. Using the charge carrier tunneling effect, graphene-based transistors can be manufactured, as shown in [1]. A theoretical overview of the properties of graphene structures can be obtained in [2]. Methods for fabrication and characterization of graphene crystals are described in [3]. The calculation of light absorption by graphene crystals in the visible range is described theoretically in [4] and confirmed experimentally in [5]. The calculation of the graphene conductivity tensor and the derivation of the plasmon dispersion law in graphene are discussed in [6].

## 2.2 Review of works on graphene ellipsometry

The results of ellipsometric measurements of graphene crystals can be found in [7]. This work raised certain questions regarding graphene ellipsometry. First,when using different graphene substrates, we obtained significantly different graphene dispersion dependences. Secondly, it became clear that the choice of a model for data analysis plays a big role. Third, it turned out that within the framework of the conventional approach to processing ellipsometric data, it is impossible to estimate the errors of the obtained values of graphene optical constants. Graphene ellipsometry was also performed in [8]. In this paper, the choice of model is also not fully understood. For example, in this paper, an intermediate layer with a Cauchy dispersion is represented between the graphene

crystal and the substrate. The authors of another paper on graphene ellipsometry [9] circumvented the problem of model selection uncertainty by searching for optical constants using the B-spline method. Nevertheless, the authors used $Si/SiO_2$ as a substrate for graphene in this study, and this, as shown in [7], can affect the observed values of the optical constants. In the paper [10], we analyzed the errors of conventional procedures for analyzing ellipsometric data. It also shows how skewed the results can be when using different assumed variance models. As an alternative, we propose an original method that allows using the ellipsometric map of a sample to measure the thickness of a thin film along with the refractive index. The errors of this method are also analyzed there, and it also shows how to minimize them. However, this method is only applicable for analyzing transparent structures.

## 2.3 Optical response models for thin films

Modification of Fresnel formulas in the case of thin film deposition was already proposed in the classic book [11]. The idea of this modification is implemented in the formulas (9), (9) of Appendix 1. In the same Appendix 1, the linear change in the ellipsometric ratio is calculated when a thin intermediate layer is added. These formulas are the first approximation for solving the problem of changing the appearance of Fresnel formulas when adding a thin intermediate layer. However, these formulas are difficult to use when analyzing experimental data, because the desired indicator is the refractive index of the film $n$ is included in them in a nontrivial way. If we consider the complex number of changes in the ellipsometric ratio $\delta\rho$ measured in the experiment, then the system of equations for the real and imaginary parts of the refractive index of the film will be quite difficult to solve. In addition, the values of the ellipsometric angles $\psi$ and $\Delta$ are obtained directly from the experiment, so there is a request to implement the perturbation theory in these variables. A simplification of this problem can be found in the linear model of the optical response of thin films proposed by in [12]. The authors of this paper propose to consider a thin film as a layer with a constant refractive index along the film thickness. Under this assumption, they also obtain linear perturbations of the reflection coefficients for both polarizations along the phase run-up inside the film. However, the calculations made in this paper should be treated with great caution. The reflection coefficients calculated by the authors of this paper differ from the true reflection coefficients by exponential phase factors. These multipliers are justified by the fact that the authors want to recalibrate reflection coefficients to the point where the reflection coefficient was measured before applying the film: at the interface with the substrate. The present reflection coefficient is measured from the outside of the thin film, and the one introduced by the authors of the article is measured from the inside. It is with these caveats that the formulas from this article should be used. Also in [12], the conditions for the applicability of a linear model are given. The approach to considering a thin film as a small perturbation of the Fresnel formulas was considered back in [13]. By the same author, based on the obtained formulas in the article [14] the inverse problem of finding the film thickness and refractive index was set and solved. But in this paper, only the case of a transparent film immersed in a homogeneous medium is analyzed. Also, in another paper, [15], this author developed a theory that allows us to calculate not only the

optical constants of the layer, but also its thickness from ellipsometric relations for the reflection and transmission coefficients, and the introduced procedure allows us to obtain solutions that are stable in terms of noise in experimental data.

# 3 Theoretical part

## 3.1 Basic concepts of ellipsometry

The basic ellipsometry equation has the form:

$$\rho = \frac{r_p}{r_s} = \text{tan}\psi\text{exp}(i\Delta) \tag{1}$$

Here, $r_s$ and $r_p$ are the reflection coefficients for $s-$ and $p-$ polarizations of light, respectively, and $\psi$ and $\Delta$ are the values measured in ellipsometry. To get information about the film, you need to compare $\psi$ and $\Delta$ in the cases before and after applying the film. To do this, it is useful to write this equation in small increments:

$$\frac{\delta r_p}{r_p} - \frac{\delta r_s}{r_s} = \frac{1}{\sin\psi\cos\psi}\delta\psi + i\delta\Delta \tag{2}$$

To the left is the difference in the relative changes in the reflection coefficients for the $s-$ and $p-$ polarizations. If we find out how this difference is expressed in terms of the optical constants of a thin film, we can make a procedure for finding solutions.

## 3.2 Transfer matrix method

If the beam falls on the same boundary between the media, the reflection and refraction coefficients are calculated using Fresnel formulas. If the beam falls on a structure with two interfaces, then the same problem is solved by the multipath reflection method, as shown in Section 7.3 [16]. For the case when there are more than two boundaries, a universal transfer matrix method is developed. This method relies on two facts. First, the electric and magnetic fields at the interfaces of media are related to each other by the usual boundary conditions. Second, differential equations describing the propagation of waves in the structure are linear. It follows that the amplitudes of electric and magnetic fields at each subsequent boundary must be expressed linearly in terms of the corresponding amplitudes at the previous boundary. The coefficients of these linear relationships can be assembled into a matrix. For a detailed derivation of the components of such a matrix for a homogeneous layer, see section 8 [16]. We need transfer matrices for a homogeneous layer in the cases of $s-$and $p-$ polarizations. At the beginning, we will write them, considering the ray's incidence on the boundary to be normal:

$$M = \begin{cases} \begin{pmatrix} \cos(\varphi) & -\frac{i}{\sqrt{\varepsilon}}\sin(\varphi) \\ -i\sqrt{\varepsilon}\sin(\varphi) & \cos(\varphi) \end{pmatrix} \\ \begin{pmatrix} \cos(\varphi) & -i\sqrt{\varepsilon}\sin(\varphi) \\ -\frac{i}{\sqrt{\varepsilon}}\sin(\varphi) & \cos(\varphi) \end{pmatrix} \end{cases} = \begin{cases} \begin{pmatrix} \cos(\varphi) & -\frac{i}{n}\sin(\varphi) \\ -in\sin(\varphi) & \cos(\varphi) \end{pmatrix}, & s-\text{polarization} \\ \begin{pmatrix} \cos(\varphi) & -in\sin(\varphi) \\ -\frac{i}{n}\sin(\varphi) & \cos(\varphi) \end{pmatrix}, & p-\text{polarization} \end{cases} \tag{3}$$

For solving optical problems, it is more convenient to write these matrices in terms of the refractive index $n$. Such a matrix, acting on a vector of dimensionless amplitudes of electric and magnetic fields at the next boundary along the beam, outputs a vector of the same amplitudes at the previous boundary. If there are several boundaries, then to get the field amplitudes at the boundary that first meets the ray, you need to act on the field amplitudes at the last boundary sequentially with the matrices of all intermediate layers. Here and further, we will assume that the ray falls from a medium with an index of refraction of $1$. Then, using the calculated amplitudes, the reflection coefficients from the boundary for both polarizations are calculated using the same formula.

$$r = \frac{u_0\cos\theta - v_0}{u_0\cos\theta + v_0} \tag{4}$$

Here $u_0, v_0$ are the found amplitudes at the first boundary of the structure, and $\theta$ is the angle of incidence of the beam on the structure.

## 3.3 Linear two-dimensional model

The equations of the linear two-dimensional model were taken from [12]. These equations allow us to calculate the relative change in the reflection coefficients when two conditions are met: normal beam incidence and a sufficiently small thickness of the deposited film. The film will be considered sufficiently thin if the phase gain in it is small. In this case, we can use the expansion of the reflection coefficients from the structure in a series with respect to a small parameter-the phase run in the film. Let's see how this limit transition is implemented. As an example, we will consider the normal incidence of a ray on a structure from our thin film with a refractive index $n$ deposited on a semi-infinite substrate with a refractive index $_s$. Both refractive indices can be complex here. The reflection coefficient from such a structure has the form:

$$r = \frac{(1-n_s)\cos\varphi - i(n_s-n^2)\,\varphi_0\,\frac{\sin\varphi}{\varphi}}{(1+n_s)\cos\varphi - i(n_s+n^2)\,\varphi_0\,\frac{\sin\varphi}{\varphi}} \tag{5}$$

Here $\varphi$ is the phase incursion in the film, and $\varphi_0$ is the corresponding phase incursion in vacuum, i.e. $\varphi = n\varphi_0$. Both of these parameters are small in the two-dimensional model. For example, a graphene film has a thickness of about $0.35\ \ textnm$, which is much smaller than the wavelength of visible light $\approx 500$nm. So, we can use the expansion of this expansion coefficient in the Taylor series to a linear term in $\varphi$. After decomposition, the relative difference of the reflection coefficients with and without film is obtained:

$$\frac{r - r_0}{r_0} = -\frac{2i(n^2 - n_{\text{sub}}^2)}{n(n_{\text{sub}}^2 - 1)}\varphi \tag{6}$$

This equation is obtained under the assumption that a thin film lies alone on an infinite substrate and that light falls on it normally. To make a universal procedure for data analysis based on it, you need to answer two questions. First, it is necessary to find out whether the same ratio applies if there is an additional film between the film and the substrate. Secondly, you need to understand what to do with this ratio if the beam incidence on the substrate is not normal, but inclined.

### 3.3.1 Linear two-dimensional model with an intermediate film

Let us consider a model with one intermediate film and calculate the relative change in the reflection coefficients in the first approximation with respect to $\varphi$. In general, we obtain a complex expression that strongly depends on the $\varphi_1$ - phase incursion in the intermediate film. However, if the intermediate film is also quite thin, then we can decompose this result by $\varphi_1$ and get the following result:

$$\frac{r - r_1}{r_1} = \left(-\frac{2i(n^2 - n_{\text{sub}}^2)}{n_{\text{sub}}^2 - 1} + \frac{4(-n_1^2 n_{\text{sub}} + n^2 n_1^2 n_{\text{sub}} + n_{\text{sub}}^3 - n^2 n_{\text{sub}}^3)}{n n_1 (n_{\text{sub}}^2 - 1)^2}\varphi_1\right)\varphi_0 \tag{7}$$

Here $r_1$ is the reflection coefficient from the medium with an intermediate film. The first term repeats the formula for the case without an intermediate film. The second term corresponds to a change in this ratio when an intermediate film is added. In the case of a sufficiently thin intermediate substrate, we can ignore the second term and use the formula in its original form.

### 3.3.2 Linear two-dimensional model in the case of oblique beam incidence

To obtain similar equations for the case of inclined beam incidence, it is necessary to reduce the case of inclined beam incidence to the case of normal incidence. Let us write out the matrices of a homogeneous layer in the case of oblique incidence for two polarizations:

$$M = \begin{cases} \begin{pmatrix} \cos(k_0 n \cos\nu d) & -\frac{i}{n\cos\nu}\sin(k_0 n\cos\nu d) \\ -in\cos\nu\sin(k_0 n\cos\psi d) & \cos(k_0 n\cos\nu d) \end{pmatrix}, & s-\text{polarization} \\ \begin{pmatrix} \cos(k_0 n \cos\nu d) & -\frac{in}{\cos\nu}\sin(k_0 n\cos\nu d) \\ -\frac{i\cos\psi}{n}\sin(k_0 n\cos\nu d) & \cos(k_0 n\cos\nu d) \end{pmatrix}, & p-\text{polarization} \end{cases} \tag{8}$$

Here $k_0$ is the wave number of the incident wave in vacuum, $\nu$ is the angle at which the wave propagates in the layer under consideration, and $d$ is the layer thickness. This matrix is multiplied together with all intermediate matrices by a vector of dimensionless amplitudes of electric and magnetic fields in a semi-infinite substrate. Following (link), for two polarizations, we represent this vector as:

$$\text{s-polarization}: \begin{pmatrix} 1 \\ \sqrt{n_{\text{sub}}^2 - \sin^2\theta} \end{pmatrix} \qquad \text{p-polarization}: \begin{pmatrix} 1 \\ \frac{\sqrt{n_{\text{sub}}^2 - \sin^2\theta}}{n_{\text{sub}}^2} \end{pmatrix} \tag{9}$$

We neglect the dependencies on the matrix parameters of all intermediate layers. Then, in order to reduce both these matrices to their analogs for the case of normal incidence, it is enough to make substitutions, as indicated in the table:

Table 1: Parameters reduced to the case of a normal drop

| | | | |
|---|---|---|---|
| $s-$ polarization | $\tilde{n} = \sqrt{n^2 - \sin^2\theta}$ | $\tilde{d} = d$ | $\widetilde{}_s = \sqrt{{}_s^2 - \sin^2\theta}$ |
| $p-$ polarization | $\tilde{n} = \frac{n^2}{\sqrt{n^2 - \sin^2\theta}}$ | $\tilde{d} = d\frac{n^2 - \sin^2\theta}{n^2}$ | $\widetilde{n_{\text{sub}}} = \frac{n_{\text{sub}}^2}{\sqrt{n_{\text{sub}}^2 - \sin^2\theta}}$ |

### 3.4 Setting the inverse problem

The problem is to find the real and imaginary parts of the refractive index of the film, knowing from the experiment the changes in the ellipsometric angles $\delta\psi$ and $\delta\Delta$ during film deposition. In this case, we substitute (2) the relative changes in the reflection coefficients calculated using a linear two-dimensional model. We obtain the following equation:

$$-2ik_0 d\left(\frac{n_s^2 - \sin^2\theta}{n_s^4 - n_s^2 + \sin^2\theta}\frac{\varepsilon^2 - n_s^2\varepsilon + n_s^2\sin^2\theta}{\varepsilon} - \frac{\varepsilon - \sin^2\theta - n_s^2}{n_s^2 - \sin^2\theta - 1}\right) = \frac{\delta\psi}{\sin\psi\cos\psi} + i\delta\Delta \tag{10}$$

This equation with the unknown $\varepsilon$ must be solved for each experimental point. As expected, when $\theta = 0$, the left side of the equation vanishes, since the difference between $s-$ and $p-$ polarizations disappears. This is a quadratic equation, so it can be calculated quite quickly.

## 4 Experimental method

### 4.1 Sample manufacturing details

Two-dimensional graphene crystals were peeled off on purified $\text{Si}/\text{SiO}_2$substrates. The substrates were first washed with acetone, isopropanol, and distilled water. After that, cleaning was performed in the oxygen chamber for 15 seconds. The prepared substrates were heated on a tile to a temperature of about 120-140 degrees, after which an adhesive tape with graphite crystals was applied to them. After another 5-10 minutes, the tape peeled off from the substrate. During peeling, the angle between the already peeled tape and the substrate was kept as small as possible. Then the substrates were carefully cleaned of glue residues during the following procedure: they were kept in warm acetone for 15 minutes at a temperature of 60 degrees, then they were kept in room-temperature acetone for another 15 minutes, then they were quickly rinsed with isopropanol and immediately the solvent residues were removed with a nitrogen blowing gun.

## 4.2 Search for single-layer crystals

Single-layer graphene crystals were initially found using an optical microscope based on image contrast. To keep the image from being too bright, the built-in AutoWhite tool was used, which turns the image into gray shades.

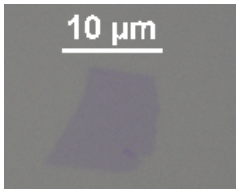


Monatomic layer

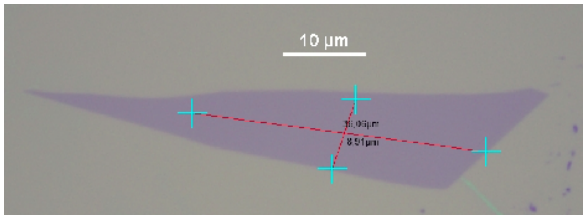


Diatomic layer

Figure 1: Graphene layers with a thickness of one and two atoms, respectively

In addition to the eye assessment, a built-in optical microscope instrument was used for preliminary sampling. This tool allows you to calculate the intensity jump based on the red, green, and blue components of light. The resulting intensity graph depends significantly on the exposure time of the microscope. Therefore, for reproducibility of the results and the possibility of comparing the obtained intensity graphs on different samples, the exposure time was fixed at $50\ textmilliseconds$, and the AutoWhite mode remained enabled.

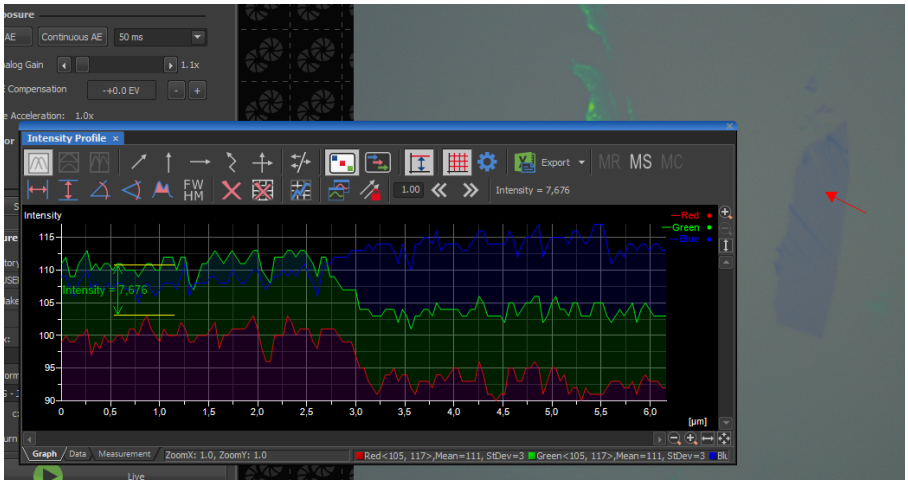


Figure 2: A jump in the intensity of the green component of light indirectly indicates that this crystal is a single-layer

## 4.3 Raman scattering

In experiments on Raman scattering on samples, a $532$ nm laser and a Horiba LabRam HR Evolution microscope were used. Graphene crystals were characterized according to citeraman by studying the position and appearance of the spectral lines G and $textrmD'$ in the Raman spectrum. These lines for graphene crystals are observed near the values of $1582$ $textcm^{-1}$ and $2700\,\mathrm{cm}^{-1}$. For single-layer and double-layer graphene layers, the peak on the G-line is lower than the peak on the D′ line, for a three-layer crystal these peaks are compared in height, and for a crystal with a large number of layers, the peak on line G is already higher than the peak on line $textrmD'$. Based on this feature, crystals with more than two layers can be effectively discarded from candidates. In this case, for single-layer crystals, the peak is located at $2678.8 \pm 1.0\,\mathrm{cm}^{-1}$, and for two-layer crystals, the peak is bifurcated and consists of two lines at $2683.0 \pm 1.5\,\mathrm{cm}^{-1}$ and $2701.8 \pm 1.0\,\mathrm{cm}^{-1}$. The presence of defects in the sample can be tracked by the height of the side peak $textrmD$.

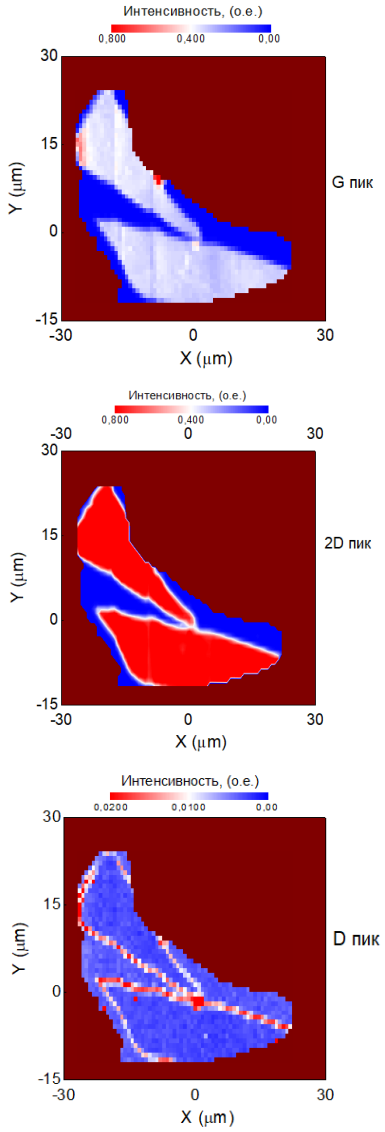


Figure 3: Raman maps with a step of $0.8$ μm obtained on graphene samples using a $3.6$ MW laser at a wavelength of $532$ nm for peaks G, D′ and D from left to right

Based on the received Fig. 3 we can conclude that this sample consists of four zones. However, the number of layers is the same for the upper and lower zones as for the left and right zones. After measuring the Raman spectrum in the centers of the regions on the left and right, we obtain graphs as shown in Fig.4:

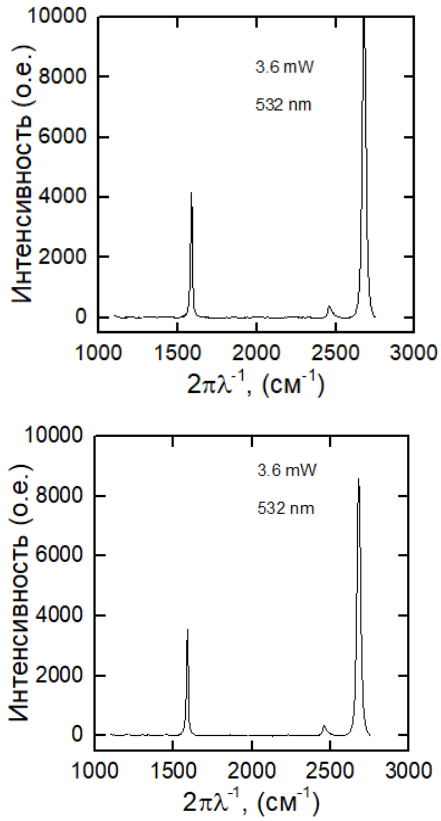


Figure 4: Raman spectra at selected points

Based on the results of measuring and comparing the scattering spectra in areas with different numbers of layers, it was confirmed that the selected candidates for single-layer crystals are indeed single-layer.

## 4.4 Atomic force microscope measurements

The crystal thickness was measured using an NT-MDT Ntegra atomic force microscope. In Fig. 5 shows an image of one of the samples obtained by atomic force microscopy. In the same Picture. 5 the value of the sample thickness jump at the boundary is approximated. From the results of this approximation, we can conclude that since the value of the thickness jump does not exceed $0.6$ nm, and the thickness of one layer is $0.35$ nm, the resulting sample passed the single-layer test.

## 4.5 Preparing for optical measurements

The $Si/SiO_2$ substrates were chosen for exfoliating graphene on them because it is convenient to quickly find hypothetical single-layer and double-layer crystals on them. However, for optical

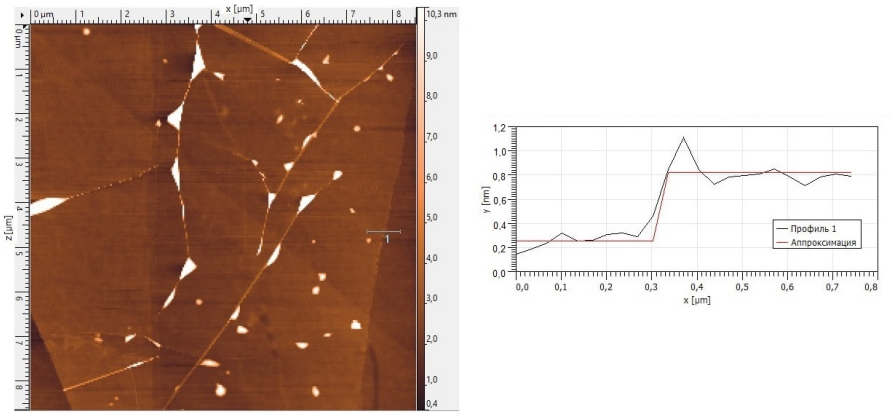


Figure 5: Left: image of the sample, right: dependence of the sample thickness at the boundary on the $x$coordinate

measurements, these substrates are not very well suited due to the fact that the absorption coefficient in the pure silicon layer significantly exceeds the absorption coefficient in the graphene layer. For this reason, the data on measuring the optical constant $k$ on graphene deposited on $\mathrm{Si}/\mathrm{SiO}_2$ are very noisy. For ellipsometer measurements, it is preferable to have a single-layer graphene crystal on glass. In this case, a thin layer of hexagonal boron nitride is placed as an intermediate layer between graphene and glass. The graphene sample adheres well to such a substrate, and all irregularities in the crystal thickness are almost perfectly smoothed out. For more information about the effect of improving the quality of a graphene sample using such a substrate, see [18]. The probability that the crystal will break away from the hexagonal boron nitride or otherwise deteriorate is minimal. If the part of the graphene crystal that is adjacent to the layer of hexagonal boron nitride was clean of all kinds of dirt when setting graphene, it will remain clean afterwards. If any dirt is found on the outside of the graphene crystal, then due to the fact that the crystal is mounted on a platform made of hexagonal boron nitride, the graphene crystal will also not deteriorate when washing the sample.

## 4.6 Transfer of crystals

6

Crystals of hexagonal boron nitride exfoliated immediately on the glass substrate. Among them, using a microscope, the largest and thinnest crystals were found without steps, defects at the edges and dirt. To lift the graphene crystal from the $\mathrm{Si}/\mathrm{SiO}_2$ substrate and lower it onto the selected crystal of hexagonal boron nitride, the manipulations shown in Fig. 6. A section of PDMS film with a thickness of about $0.5\ textmm$ and a length and width of about $3$ mmwas placed on the slide near the edge. The glass with PDMS film was then baked on the tile at a temperature of 150 degrees. The polycarbonate (PC) film was prepared in advance according to this procedure. $0.06$ of dry polycarbonate was filled to about $1.05\ textg$ by weight with chloroform and left to stir for $12$ h with a magnetic stirrer under the hood. The resulting liquid was dripped onto one slide, after which a thin film was formed on both slides by moving the second slide. From the glass, this polycarbonate was

lifted with tape with a pre-made hole, in length and width slightly larger than the size of the PDMS film. With this adhesive tape, the polycarbonate film was stretched over the PDMS film, trying to achieve an even tension of the polycarbonate. The resulting glass with stretched polycarbonate was again baked at a temperature of 150 degrees. This glass was inserted into the manipulator of the transfer machine.

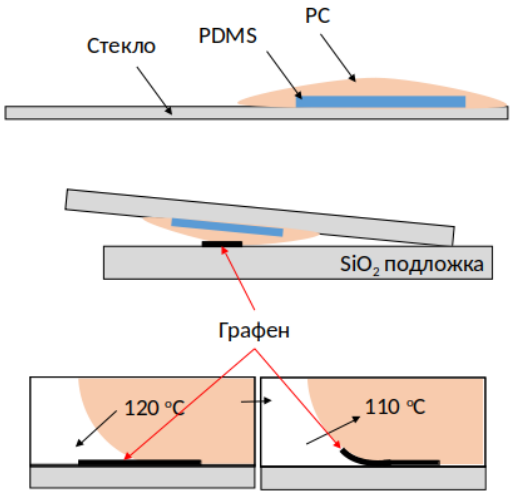


Figure 6: Graphene lifting scheme

Graphene was lifted from $mathrmSi/\mathrm{SiO_2}$ to a region of polycarbonate with a minimum number of cracks at a temperature of $100 - 120$ degrees by a sharp movement of the transfer machine table. Graphene was lowered onto hexagonal boron nitride at a temperature of about $120$ degrees.

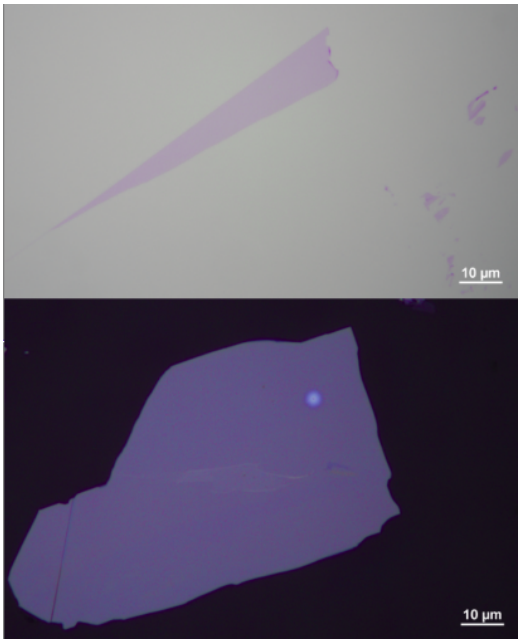


Figure 7: From top to bottom: graphene on $mathrmSi/\mathrm{SiO_2}$, graphene on hexagonal boron nitride on glass

## 4.7 Ellipsometry of samples

Ellipsometric maps were measured for those crystals that were confirmed to be single-layered. We used an Accurion EP4 ellipsometer. For the measurements, the method of spectral ellipsometry was chosen according to the scheme with a rotating compensator, as shown in Fig. 8.

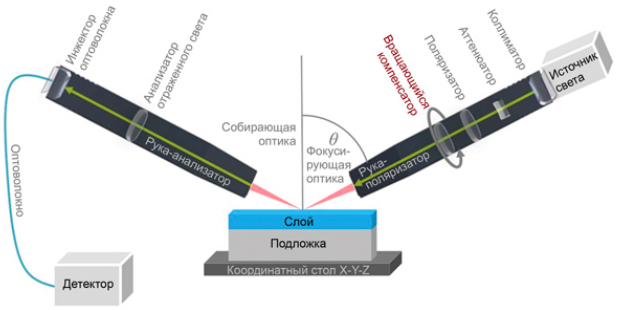


Figure 8: Ellipsometer operation diagram, image from the site dipaul.ru

The measurements were performed using the knife edge illumination technology, the diagram of which is shown in Fig. 9. Part of the light beam is cut off just before it hits the sample. Because of this, the beam splits in reflected light: in one of its parts, there is no reflection from the back surface of the substrate. Analyzing this particular part of the beam, we can assume that the back surface of the substrate is semi-infinite.

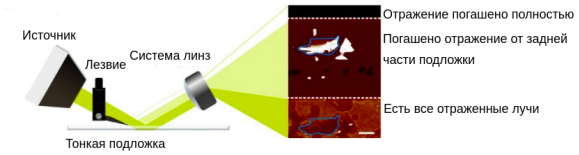


Figure 9: How the knife edge illumination technology works, image taken from [19]

One pixel in the ellipsometer operation corresponds to an area of $0.01\ \ textmicrons^2$. To successfully take readings on the ellipsometer, you need to get a sample whose area with an indent from the edges and various defects will exceed about $50\ \ textmicrons^2$. This condition is necessary to collect sufficiently reliable statistics for $psi$ and $\Delta$ and to suppress noise as much as possible. It is advantageous to make measurements at angles close to the Brewster angle, but this reduces the area scanned by the ellipsometer beam. To balance the impact of these factors, ellipsometry was taken for three different angles of incidence: $52,\ 55$, and $58$ degrees. The time of signal accumulation by the detector is controlled programmatically. The detector picks up light until it is saturated, until it enters overload mode. The results of measurements of ellipsometric angles $\psi$ and $\Delta$ for a single-layer graphene crystal are shown in the graph.

According to the graphs in Fig. 10 it can be seen that applying a thin graphene film, as expected, has very little effect on the ellipsometer reading.

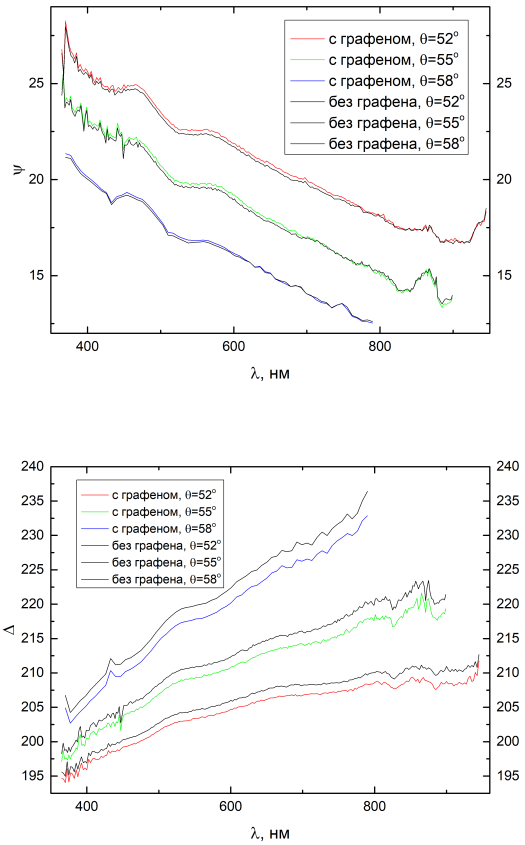


Figure 10: Measured wavelength dependences of $psi$ and $\Delta$

# 5 Analysis of experimental data

## 5.1 Dealing with systematic errors

Data for each area measured using an ellipsometer is averaged over several thousand points. Analysis of the statistical relationship between these measurements shows that the response values are normally distributed, which means that with a sufficiently large number of measurements, we can reduce the statistical spread with the accuracy we need. However, there is a source of systematic error in the experimental scheme that significantly affects the measurement results. This is an imperfect alignment of the optical system. This imperfection can be observed directly: through the crossed polarizer and analyzer, the signal still arrives. This factor provides some shift in the measured ellipsometric ratio $rho$:

$$\rho_{\text{exp}} = \rho_{\text{ideal}} + \delta\rho_{\text{shift}} \tag{11}$$

In turn, the effect of applying a thin film can also be considered in a linear approximation as a shift of the measured ellipsometric ratio by the corresponding value of $delta\rho_{\text{gr}}$.

$$\rho_{\text{exp, gr}} = \rho_{\text{ideal}} + \delta\rho_{\text{shift}} + \delta\rho_{\text{gr}} \tag{12}$$

A big problem for analyzing ellipsometric data using models is the fact that $\delta\rho_{\text{gr}}\ sim\delta\rho_{\text{shift}}$. You can't embed $\delta\rho_{\text{shift}}$ in the optical model. It can only explain $\rho_{\text{ideal}}$. Thus, it turns out that if we directly analyze data from graphene on a substrate, the interpretation of the results obtained cannot claim to be highly accurate. In this regard, the idea arises: to make measurements and get the values corresponding to the formulas $(5.1)$ and $(5.1)$ for all experimental points. The systematic error resulting from imperfect alignment can be taken into account by subtracting the model values from the experimental values in $(5.1)$:

$$\rho_{\text{exp, gr}} = \rho_{\text{ideal}} + (\rho_{\text{exp}} - \rho_{\text{ideal}}) + \delta\rho_{\text{gr}} \tag{13}$$

In this formula, $\rho_{\text{exp}} - \rho_{\text{ideal}}$ should be a column of correction numbers obtained as a result of an experiment without an additional thin film, and the first term $\rho_{\text{ideal}}$ should already be subjected to optimization procedures.

## 5.2 Calculations using the Drude-Lorentz model

First of all, graphene ellipsometry data were processed according to the conventional procedure. As an optical model of a thin layer, graphene was assumed to be a homogeneous layer with a thickness of $0.335$ nm with a Drude-Lorentz dispersion relation.

$$\varepsilon = 1 - \frac{\hbar^2}{\varepsilon_0\rho(\tau E^2 + i\hbar E)} + \frac{A_L B_L E_L}{E_L^2 - E^2 - iB_L E} \tag{14}$$

Five parameters of this model - resistivity $rho$, free path time $\tau$, amplitude, width, and position of the resonance $A_L$, $B_L$, and $E_L$ - were optimally selected as a result of the Levenberg-Mcwardt algorithm, which finds a local minimum for the error function corresponding to this problem. The experiment was performed on two graphene samples. The first crystal was peeled off and placed on a glass substrate. The second sample was obtained by chemical vapor deposition (CVD). The difference between these samples can be seen from Fig. 11, rather thin. The optical constants of detached graphene over the entire wavelength range under study are larger than the optical constants of graphene CVD. It is important that this result was obtained only after applying the procedure described in equation (13). Thus, the accuracy of work within the framework of the model approach can be significantly increased using this procedure. This approach is described in more detail in [20].

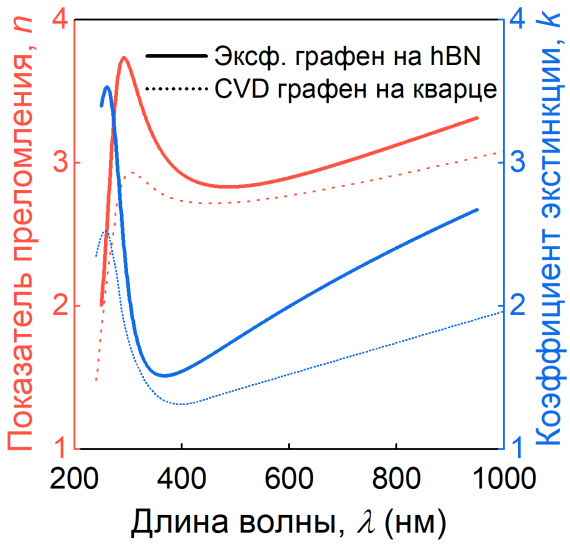


Figure 11: Dispersion of optical constants of exfoliated graphene and CVD graphene

## 5.3 Calculations using analytical formulas

Three different situations were considered in the calculations. First, we studied the operation of the program in the case of neglecting the contribution of the intermediate layer of hexagonal boron nitride in accordance with the formula (10). Second, the intermediate layer was taken into account according to the linear decompositions (9) and (9). In this case, such considerations were used to compare the reflection coefficients exactly before and after graphene deposition:

$$r_{12} = r_0(1 + g_{12}), \quad r_1 = r_0(1 + g_1), \quad \frac{r_{12} - r_1}{r_1} = \frac{g_{12} - g_1}{1 + g_1} \tag{15}$$

Here $g$ is responsible for linear corrections to the reflection coefficients, the presence of index 1 means that this reflection coefficient is calculated from a system without graphene, but with boron nitride, and the presence of indices 1 and 2 together means that this reflection coefficient corresponds to a system with both boron nitride and graphene.

Finally, the intermediate layer was considered in the framework of the formulas of Appendix 1, but without linear expansion of the coefficients. The calculations used data on the dispersion of glass and hexagonal boron nitride, and in the second and third situations, the anisotropy of the intermediate layer was taken into account in the form of corresponding corrections to $q$ and $p$ according to (9). Calculations were performed using Wolfram Mathematica. The data files and the program used for analysis can be found at `https://github.com/begichev/ThinFilmEllipsometry`. SolverEpsilon.nb script with the specified coefficient The refractive index of the substrate, the angle of incidence of light, and the thickness of the two-dimensional material layer are solved by the equation (10) for all experimental points. As a result of the script, text files with calculated dependences of optical constants on the wavelength appear in the optconsts folder, and graphs of these dependencies are placed in the plots folder. The dependencies for different angles looked almost identical, and it

was decided to average them over the corners. To do this, the Merge.nb script was used, which takes the calculated optical constants from the optconsts folder and averages them using this algorithm:

- Build a common scale-combining all values of $lambda$ for which experimental data were measured for at least one angle
- For each point of the resulting general scale, find two nearest neighbors from the scales corresponding to each of the three corners. For each pair of neighbors, average the result with the weight inverse to the modulus of the distance on the scale:

n = n˙1 —$\lambda - \lambda_2|+n_2|\lambda - \lambda_1|_{\overline{|\lambda-\lambda_1|+|\lambda-\lambda_2|}}$
(16)

Based on the obtained three values of the nearest neighbor averages, now take the arithmetic mean. Write it down in accordance with the point of the general scale.

# 6 Results and discussion

## 6.1 Accounting for an intermediate layer

By looking at the Pic. 12, we can conclude that the linear approximation for the intermediate layer of hexagonal boron nitride generally behaves similarly to other computational procedures, but has significant deviations at small wavelengths. This can be explained by the fact that although the thickness of the intermediate layer in the experiment $30\text{nm}$ was much smaller than the wavelength, the small parameter should have been the phase gain in the intermediate layer $phi_1$. Given that hexagonal boron nitride has $n \approx 5$, we get $\varphi_1 \approx \frac{150\,\text{nm}}{\lambda}$. This value can no longer be considered small, especially at small wavelengths, where the differences are most pronounced. However, if we take into account non-linear corrections from the intermediate layer, the result becomes very similar to that observed when the intermediate layer is completely neglected. It turns out that in this situation, not taking into account the intermediate layer in any way is better than taking it into account poorly. This point of view is also confirmed by numerical experiments that ignored the anisotropy and dispersion of the optical constants of the intermediate layer. All of these experiments produced poor results that did not agree with common sense and the results obtained by other methods.

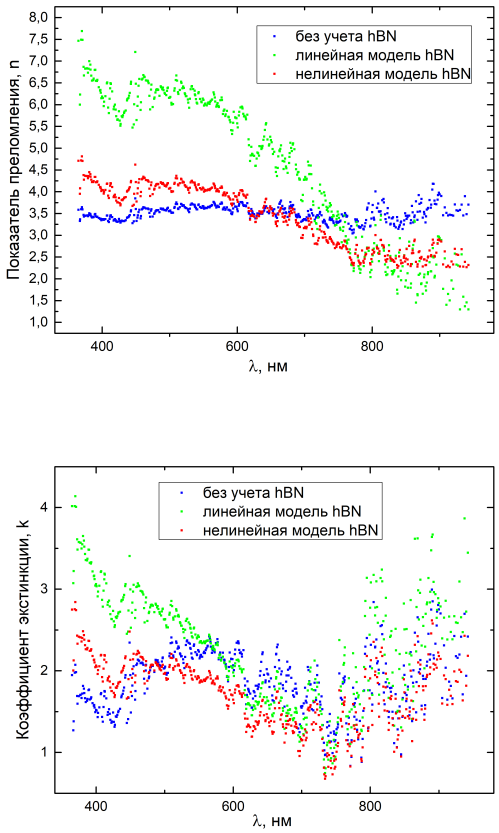


Figure 12: Calculated dependences of$n$and$k$ on the wavelength

## 6.2 Comparison with the results obtained using the model

By comparing the dependencies from Fig. 12 and Fig. 11, you can make the following observations:

- In both figures, the variance of the refractive index $n$ is not very significant in the range under study; the refractive index itself is approximately $3.5$. The small positive slope of the dependence obtained in Fig. 11, not reproduced in Fig. 12

  At the same time, the variance of the extinction coefficient is quite significant. Both figures show the growth of $k$ from $1$ to $3.5$ on the test range

## 6.3 Comparison with the results obtained by other authors

The obtained variance dependences can be compared with the results of previous studies. First, the results of [7] were not confirmed in this experiment. According to the authors ' conclusions, both the real and imaginary parts of the refractive index should sharply increase by 3-4 times in the studied range, which is not observed in Fig. 12. The results of this work are in much better agreement with those provided in citeGrBSplined: both characteristic maxima of optical constants in the wavelength region $\lambda = 300\ textnm$ are well reproduced both there and in Fig. 11, and the other

parameters of the dispersion curves also match very well.

### 6.4 Discussion

The results of this work could be refined and improved. It would be useful, for example, to calculate errors in places where this is possible. It would be worth starting with the corrected Fresnel formulas from Appendix 1, determining with what accuracy the formulas for reflection coefficients are performed according to the phase run-up in the film, if linear approximation is not applied to them. Also noteworthy is the coarsening that was allowed in the calculation of the integrals $q$ and $p$. The form of the function $eps(z)$ on the scale of the integration segment remains unknown. In this case, we can come up with models of the effective parameters responsible for the graphene response, as, for example, was done in citeef˙param. With this approach, it would be necessary, for example, to recalculate the thickness of the graphene layer to new effective values.

## 7 Conclusions

In thin film ellipsometry, there are many problems related to measurement accuracy. In this paper, two ways of dealing with these problems are considered and applied. Both of these methods are applicable in such an experiment, where it is possible to measure the ellipsometry of the system before applying the next thin film and after applying it. The first method is designed to deal with systematic errors. For a system with a well-known theoretical response, it is possible to obtain contributions to $\psi$ and $\Delta$ from experimental data obtained on it, which are related to the inaccuracy of alignment. These deposits can then be deducted when applying regression analysis to an optical model of a system with a deposited film. This is how the results were obtained in Fig. 11. The second method is also ideologically aimed at eliminating the influence of systematic inaccuracies in the processing of measurements. Equations of the type (10) and similar models allow us to obtain the optical constants of the deposited film, using not the measured $\psi$ and $\Delta$ themselves, but their differences. An important difference between the second method and the first is that in this case the optical constants are expressed by an analytical equation in terms of experimental data. data. For example, the equation (10), which showed a fairly good agreement with the refined model, is quadratic, which means that its solutions are expressed explicitly in terms of experimental data. This allows you to calculate their errors for the results obtained. This method can work when analyzing heterostructures from a large number of layers if ellipsometry data is available before and after applying the next layer. Another advantage is that the analysis method easily integrates information about the anisotropy of layers of the standard type (9).

# 8 Acknowledgements

I would like to express my gratitude to my colleagues from the Center for Photonics and Two - dimensional Materials at MIPT-Adilet Toksumakov for their great support in fabricating samples and experiments, Georgy Ermolaev for their help in mastering the ellipsometer, Natalia Doroshina for her help in making Raman scattering maps, Dmitry Yakubovsky for their support in working with the atomic force microscope, and my scientific assistant to the supervisor David Armenovich Ghazaryan for valuable advice on the design of the work.

# References


[1] T. L. Lane, J. R. Wallbank, V. I. Fal'ko. Twist-controlled resonant tunnelling between monolayer and bilayer graphene. Appl. Phys. Lett. (2015)

[2] M. I. Katznelson. The Physics of Graphene, 2nd edition. Cambridge university press. (2020)

[3] E. Khestanova. Van der Waals Heterostructures: Fabrication, Mechanical and Electronic Properties. Doctor thesis (2017)

[4] L.A. Falkovsky. Optical properties of graphene. Journal of Physics: Conference Series 129 (2008)

[5] K. F. Mak, M. Y. Sfeir, Y. Wu. Measurement of the Optical Conductivity of Graphene. Phys. Rev. (2008)

[6] L.A. Falkovsky, A.A. Varlamov. Space-time dispersion of graphene conductivity. The European Physical Journal B. (2007)

[7] U. Wurstbauer, C. Röling, et. al. Imaging ellipsometry of graphene. Applied Physics Letters (2010)

[8] V. G. Kravets, A. N. Grigorenko, R. R. Nair, P. Blake, S. Anisimova, K. S. Novoselov, A. K. Geim. Spectroscopic ellipsometry of graphene and an exciton-shifted van Hove peak in absorption. Phys. Rev. (2010)

[9] J. W. Weber, V. E. Calado, M. C. M. van de Sanden. Optical constants of graphene measured by spectroscopic ellipsometry. Appl. Phys. Lett. (2010)

[10] P. Nestler, C. A. Helm. Determination of refractive index and layer thickness of nm-thin films via ellipsometry. Optics express (2017)

[11] P. Drude, C. R. Mann, R. A. Millikan. The theory of optics. New York : Longmans, Green, and Co. (1902)

[12] Y. Li, T. Heinz. Two-dimensional models for the optical response of thin films. 2D Mater (2018)

[13] J. Lekner. Ellipsometry of surface films on a uniform layer. Journal of the Optical Society of America (1988)

[14] J. Lekner. Analytic inversion of ellipsometric data for an unsupported nonabsorbing uniform layer. Journal of the Optical Society of America (1990)

[15] J. Lekner. Determination of complex refractive index and thickness of a homogeneous layer by combined reflection and transmission ellipsometry. Josa communications (1994)

[16] O. Stenzel. The Physics of Thin Film Optical Spectra. An Introduction. (2016)

[17] D. Graf, F. Molitor, K. Ensslin, C. Stampfer, A. Jungen, C. Hierold, L. Wirtz. Spatially Resolved Raman Spectroscopy of Single- and Few-Layer Graphene. Nano Letters (2007)

[18] C. R. Dean, A. F. Young, I. Meric. Boron nitride substrates for high-quality graphene electronics

[19] S Funke, B Miller, E Parzinger. Imaging spectroscopic ellipsometry of $\mathrm{MoS_2}$. J. Phys.: Condens. Matter (2016)

[20] M. A. El-Sayed,, G. A. Ermolaev, K. V. Voronin. Optical constants of chemical vapor deposited graphene for photonic applications. Nanomaterials (2021)

[21] J. Fang, W. G. Vandenberghe, M. V. Fischetti. Microscopic dielectric permittivities of graphene nanoribbons and graphene. Phys. Rev. (2016)

# 9 Appendix 1. Influence of the intermediate layer on Fresnel formulas

There are two media with permittivity $eps_1$ and $\varepsilon_2$. If the boundary between them is a line of zero thickness, Fresnel formulas are used to find the reflection and transmission coefficients. Let us consider a slightly different case: let the boundary between these two media be an optically thin intermediate layer. In this case, we will keep only the linear terms in the expansion with respect to a small parameter-the wave phase arrival in the intermediate layer. We introduce the coordinate axes: the $oZ$ axis is across the media boundary, so $oXZ$ is the plane of incidence. We introduce the angles $alpha_i$, $\alpha_r$, and $\alpha_t$ between the wave vectors of the incident, reflected, and refracted waves and the positive direction of the $oZ$axis. Then the wave vectors of these waves are written as follows:

$$\overline{k_i} = k_1 \begin{pmatrix} \sin\alpha_i \\ 0 \\ \cos\alpha_i \end{pmatrix} = k_1\overline{n_i}, \quad \overline{k_r} = k_1 \begin{pmatrix} \sin\alpha_r \\ 0 \\ \cos\alpha_r \end{pmatrix} = k_1\overline{n_r}, \quad \overline{k_t} = k_2 \begin{pmatrix} \sin\alpha_t \\ 0 \\ \cos\alpha_t \end{pmatrix} = k_2\overline{n_t} \tag{17}$$

Here $k_1 = \frac{\omega}{v_1}$, $k_2 = \frac{\omega}{v_2}$. In this case, $v_1$, $v_2$ are the wave propagation velocities in the first and second media. The magnetic field in a wave is related to the electrical relation $H = \sqrt{\varepsilon}\,\overline{n} \times \overline{E}$. Knowing all this, we write down the vectors of incident, reflected, and refracted waves. In this case, the lower index $p$ will indicate the components of the electric field in the plane of incidence, and the index $s$ - in the perpendicular direction along the $oY$ axis.

$$\overline{E_i} = \begin{pmatrix} E_p^{(i)}\cos\alpha_i \\ E_s^{(i)} \\ -E_p^{(i)}\sin\alpha_i \end{pmatrix} \exp\Big(i\omega t - i\tfrac{\omega}{v_1}(x\sin\alpha_i + z\cos\alpha_i)\Big) \tag{18}$$

$$\overline{H_i} = \begin{pmatrix} -E_s^{(i)}\cos\alpha_i \\ E_p^{(i)} \\ E_s^{(i)}\sin\alpha_i \end{pmatrix} \exp\Big(i\omega t - i\tfrac{\omega}{v_1}(x\sin\alpha_i + z\cos\alpha_i)\Big) \tag{19}$$

$$\overline{E_r} = \begin{pmatrix} E_p^{(r)}\cos\alpha_r \\ E_s^{(r)} \\ -E_p^{(r)}\sin\alpha_r \end{pmatrix} \exp\Big(i\omega t - i\tfrac{\omega}{v_1}(x\sin\alpha_r + z\cos\alpha_r)\Big) \tag{20}$$

$$\overline{H_r} = \begin{pmatrix} -E_s^{(r)} \cos\alpha_r \\ E_p^{(r)} \\ E_s^{(r)} \sin\alpha_r \end{pmatrix} \exp\left(i\omega t - i\frac{\omega}{v_1}(x\sin\alpha_r + z\cos\alpha_r)\right) (21)$$

$$\overline{E_t} = \begin{pmatrix} E_p^{(t)} \cos\alpha_t \\ E_s^{(t)} \\ -E_p^{(t)} \sin\alpha_t \end{pmatrix} \exp\left(i\omega t - i\frac{\omega}{v_1}(x\sin\alpha_t + z\cos\alpha_t)\right) (22)$$

$$\overline{H_t} = \begin{pmatrix} -E_s^{(t)} \cos\alpha_t \\ E_p^{(t)} \\ E_s^{(t)} \sin\alpha_t \end{pmatrix} \exp\left(i\omega t - i\frac{\omega}{v_1}(x\sin\alpha_t + z\cos\alpha_t)\right)$$

(23)

If there were no intermediate layer, then the boundary conditions would be as follows: the components of the fields along the $oX$ and $oY$ axes on both sides of the boundary must be equal. If we use this, we get the Fresnel formulas:

$$\text{r˙p0} = \cos\alpha_i \overline{n_1 - \frac{\cos\alpha_t}{n_2}} \overline{\frac{\cos\alpha_i}{n_1} + \frac{\cos\alpha_t}{n_2}}, \quad r_{s0} = \frac{n_1\cos\alpha_i - n_2\cos\alpha_t}{n_1\cos\alpha_i + n_2\cos\alpha_t}$$

(24)

Now we are interested in how the boundary conditions change in the presence of an intermediate layer. We will use the assumption $\overline{D}here = \ eps\overline{E}$, that is, consider the film isotropic. This is only done for ease of computation. If necessary, you can add anisotropy to the model at this point and get formulas that correspond to this case. It is intuitively clear that if the tangential components of the fields were equal to each other in the consideration without an intermediate layer, then when the film is added, they should be equal with a small correction. To calculate this correction: we write down those Maxwell equations that contain derivatives in the $oZ$ direction of the tangential components of the fields. After integrating in the $oZ$ direction, we obtain corrected boundary conditions.

$$1\overline{c\frac{\partial H_y}{\partial t} = \frac{\partial E_z}{\partial x} - \frac{\partial E_x}{\partial z}}, (25)$$

$$1\overline{c\frac{\partial H_x}{\partial t} = \frac{\partial E_y}{\partial z} - \frac{\partial E_z}{\partial y}}, (26)$$

$$\varepsilon\overline{c\frac{\partial E_y}{\partial t} = \frac{\partial H_x}{\partial z} - \frac{\partial H_z}{\partial x}}, (27)$$

$$\varepsilon\overline{c\frac{\partial E_x}{\partial t} = \frac{\partial H_z}{\partial y} - \frac{\partial H_y}{\partial z}}$$

(28)

The derivatives with respect to $y$ in the film are zero, since the wave propagates in the $oXZ$plane. The tangential components of the fields, as well as their time derivatives, will be taken as the sign of the integral in a linear approximation. The components of the fields in the $z$ direction will be integrated, taking into account the boundary conditions on the normal components of the vectors $olD$ and $\overline{B}$. As a result, we obtain four corrected boundary conditions:

$$\begin{aligned}
&\mathrm{E}\dot{}\mathrm{x}\hat{}(1) = \mathrm{E}\dot{}\mathrm{x}\hat{}(2) + \mathrm{l}\frac{}{c\frac{\partial H_y^{(2)}}{\partial t} - \varepsilon_2 \frac{\partial E_z^{(2)}}{\partial x} q,}\\
&\mathrm{E}\dot{}\mathrm{y}\hat{}(1) = \mathrm{E}\dot{}\mathrm{y}\hat{}(2) - \mathrm{l}\frac{}{c\frac{\partial H_x^{(2)}}{\partial t},}\\
&\mathrm{H}\dot{}\mathrm{x}\hat{}(1) = \mathrm{H}\dot{}\mathrm{x}\hat{}(2) - \mathrm{l}\,\partial H_z^{(2)}\frac{}{\partial x - \frac{p}{c}\frac{\partial E_y^{(2)}}{\partial t},}\\
&\mathrm{H}\dot{}\mathrm{y}\hat{}(1) = \mathrm{H}\dot{}\mathrm{y}\hat{}(2) + \mathrm{p}\frac{}{c\frac{\partial E_x^{(2)}}{\partial t}}
\end{aligned}$$

Here, superscript 1 marks the fields in the first environment, and superscript 2 marks the fields in the second. Correction terms are written in terms of fields in the second medium to simplify calculations, since in the second medium there is only a refracted wave. The thickness of the intermediate layer is denoted as $l$. Integrals are also introduced:

$$\int_0^l \frac{dz}{\varepsilon(z)} = q, \quad \int_0^l \varepsilon(z)dz = p$$

(29)

After solving these equations in the first order by the phase run-up in the film $fracωlc$, we obtain linear perturbations of the reflection coefficients for both polarizations:

$$\mathrm{r}\dot{}\mathrm{p} = \mathrm{r}\dot{}\mathrm{p}0\left(1 + 2i\frac{\omega}{c}\cos\alpha_i\sqrt{\varepsilon_1}\frac{p\cos^2\alpha_t - \varepsilon_2 l + \varepsilon_2^2 q\sin^2\alpha_t}{\varepsilon_2\cos^2\alpha_i - \varepsilon_1\cos^2\alpha_t}\right)$$

(30)

$$\mathrm{r^{\cdot}s} = \mathrm{r^{\cdot}s0}\left(1 + 2i\frac{\omega}{c}\cos\alpha_i\sqrt{\varepsilon_1}\frac{\varepsilon_2 l - p}{\varepsilon_1\cos^2\alpha_i - \varepsilon_2\cos^2\alpha_t}\right) \tag{31}$$

To go further and get a formula for the linear perturbation of the ellipsometric relation, you need to add assumptions about the form of the function $eps(z)$ to calculate the integrals $q$ and $p$. The roughest way, which is usually used for calculations , is to imagine that this function behaves as a constant on the interval from $0$ to $l$, ignoring its interpolation to the values of $eps_1$ and $\varepsilon_2$ at the ends of the interval. In this approximation, we obtain the following formula for $rho$:

$$\rho \approx \rho_0 + i\rho'\frac{\omega l}{c} \tag{32}$$

$$\rho' = -2\frac{n_1}{n_2^2 - n_1^2}\frac{\sin^2\alpha_i\cos\alpha_i}{\cos^2(\alpha - \alpha_t)}\frac{(n^2 - n_1^2)(n^2 - n_2^2)}{n^2} \tag{33}$$

And for the reflection coefficients, we get the result in the form (6). It is convenient to get the result for normal beam incidence, and then make substitutions in accordance with the 1 Table. However, this can only be done in the isotropic case. If we reject the assumption that the film is isotropic, then we must use the formulas (9) and (9). In this case, in the sense of the introduced integrals $q$ and $p$ for a homogeneous film, they will be equal to:

$$\mathrm{q} = \mathrm{l}\overline{n^2_{\mathrm{out}},\quad p = n^2_{\mathrm{in}}\, l} \tag{34}$$

Here $n_{\mathrm{in}}$ and $n_{\mathrm{out}}$ are the refractive indices of the material in the $oXY$ plane and along the $oZ$axis, respectively.